PCCP

Dipolar motions and ionic conduction in an ibuprofen derived ionic liquid

Journal:	*Physical Chemistry Chemical Physics*
Manuscript ID:	CP-ART-06-2015-003715.R1
Article Type:	Paper
Date Submitted by the Author:	05-Aug-2015

Complete List of Authors:	Viciosa, Teresa; Instituto Superior Técnico, Universidade de Lisboa, CQFM - Centro de Química-Física Molecular and IN - Institute of Nanoscience and Nanotechnology Santos, Gonçalo; Nova University of Lisbon, FCT/LAQV REQUIMTE, Chemistry Costa, Alexandra; Nova University of Lisbon, FCT/LAQV REQUIMTE, Chemistry Danède, Florence; Université Lille1, Unité Matériaux et Transformations (UMR CNRS 8207) Branco, Luis; Nova University of Lisbon, FCT/LAQV REQUIMTE, Chemistry Jordão, Noémi; REQUIMTE, FCT/UNL, Chemistry Correia, Natália; Nova University of Lisbon, FCT/LAQV REQUIMTE, Chemistry; Université Lille1, Unité Matériaux et Transformations (UMR CNRS 8207) Dionísio, Madalena; Nova University of Lisbon, FCT/LAQV REQUIMTE, Chemistry

Physical Chemistry Chemical Physics

Received 00th January 20xx,
Accepted 00th January 20xx
DOI: 10.1039/x0xx00000x

www.rsc.org/

Dipolar motions and ionic conduction in an ibuprofen derived ionic liquid

M. T. Viciosa,[a] *G. Santos,[b] A. Costa,[b] F. Danède,[c] L. C. Branco,[b] N. Jordão,[b] N. T. Correia[b,c] and M. Dionísio[b]

It was demonstrated that the combination of the almost water insoluble active pharmaceutical ingredient (API) Ibuprofen with the biocompatible 1-ethanol-3-methylimidazolium [C_2OHMIM] cation of an ionic liquid (IL) originates a highly water miscible IL-API with a solubility increased by around 5 orders of magnitude. Its phase transformations, as crystallization and glass transition, are highly sensitive to the water content, the latter shifting to higher temperatures upon dehydration. By dielectric relaxation spectroscopy the dynamical behavior of anhydrous [C_2OHMIM][Ibu] and with 18.5 and 3% of water content (w/w) was probed from well below the calorimetric glass transition (T_g) up to the liquid state. Multiple reorientational dipolar processes were detected which become strongly affected by conductivity and electrode polarization near above T_g. Therefore [C_2OHMIM][Ibu] exhibits mixed behavior of a conventional molecular glass former and an ionic conductor being analysed in this work through conductivity, electrical modulus and complex permitivity. The dominant process, $\sigma\alpha$-process, is originated by a coupling between both charge transport and dipolar mechanisms. The structural relaxation times were derived from permittivity analysis and confirmed by temperature modulated differential scanning calorimetry. The temperature dependence of the β-secondary relaxation is coherent with a Johari-Goldstein (β_{JG}) process as detected in conventional glass formers.

I. Introduction

There is a demand in the pharmaceutical industry for the development of alternative drug formulations with increased solubility and therefore enhanced bioavailability, improving their therapeutic efficacy. Indeed, a significant number of currently marketed compounds (~40%)[1] and the majority of novel drug candidates (75%)[2] remain poorly water-soluble. A solution for this hurdle, in order to obtain highly soluble and permeable compounds, since solubility and permeability are key factors that govern drug absorption, [3] is to promote ion-pair formation enhancing the transport through membranes.[4] In this context, ionic liquids (IL) offer the possibility of simultaneously render the active ingredient principle (API) higher soluble and permeable. This can be achieved by intrinsically combining the IL with the API, preserving the API bioactivity or even undergoing a novel effect when both counter ions exhibit therapeutic activity.[5] This application results from the fact that about half of APIs are salts being possible pairing it with IL counterions and therefore tuning the IL-API properties by appropriated design and choice of ions. This falls in the designation of third generation ILs.[5,6] There are a few examples of these 'combination salts' using two actives in a single compound *e.g.* involving the anion Ibuprofenate and the IL cation didecyldimethylammonium, the former being anti-inflammatory and the latter antibacterial.[7]

In this work the almost water insoluble API ibuprofen[8], and the hydrophilic [9] and biocompatible [10] IL 1-ethanol-3-methylimidazolium hydroxide ([C_2OHMIM]OH) were intrinsically combined to form the desired salt indicated as [C_2OHMIM][Ibu] (1-ethanol-3-methylimidazolium Ibuprofenate), which is here characterized by differential scanning calorimetry (DSC), polarized optical microscopy (POM) and dielectric relaxation spectroscopy (DRS).

By solid state NMR it was observed that the dynamic properties between the acidic and the Na-salt form of ibuprofen are significantly different. In particular, in the salt, the motions of the phenyl ring become much faster and the isobutyl group experiences fast rotation while being frozen in the acidic form,[11] which is a

[a] CQFM – Centro de Química-Física Molecular and IN – Institute of Nanoscience and Nanotechnology, Instituto Superior Técnico,Universidade de Lisboa, Avenida Rovisco Pais, 1049-001 Lisboa, Portugal teresaviciosa@ist.utl.pt
[b] REQUIMTE/CQFB, Departamento de Química, Faculdade de Ciências e Tecnologia,Universidade Nova de Lisboa, 2829-516 Caparica, Portugal.
[c] Unité Matériaux Et Transformations (UMET), UMR CNRS 8207, UFR de Physique, BAT P5, Université Lille Nord de France, F-59655 Villeneuve d'Ascq Cedex, France
Electronic Supplementary Information (ESI) available: [details of any supplementary information available should be included here]. See DOI: 10.1039/x0xx00000x

promissory result for the use of ibuprofenate in the here tested IL_API. DRS allows to significant extend the frequency range in which the dynamical behaviour is probed being the major technique used in the present work.

In a typical DRS experiment, the sample is placed between two parallel electrodes being submitted to an oscillating electrical field, allowing probing dipolar polarization through the reorientational movements of dipoles, interfacial polarization and propagation of mobile charge carriers. The charge carrier's migration is due to translational diffusion through hopping movements of electrons, holes and ions giving rise to conductivity from which information on charge transport properties is obtained. While dipolar reorientations are usually probed through the complex dielectric function, $\varepsilon^*(\omega)$, conductivity is monitored by the complex electric conductivity $\sigma^*(\omega) = \sigma'(\omega) + i\sigma''(\omega)$, where σ´ and σ´´ are the corresponding real and imaginary parts. The two properties are related by $\sigma^*(\omega) = i\omega\epsilon_0\epsilon^*(\omega)$.[12] Moreover to allow the characterization of relaxation processes highly masked by conductivity as occurs in ionic materials, the spectral analysis can be made based on the complex electric modulus (M*) formalism,[13,14] which is defined as the reciprocal of the complex permittivity $M^*(\omega) = 1/\epsilon^*(\omega)$.[15,16,17] This provides a mean to access the dynamical behaviour of the compound under study, a requisite to infer about its stability upon thermal treatment and under storage. Furthermore, it allow to shed some light on the origin of the relaxational mode behind each detected process, particularly the glass transition, a phenomenon which physical origin, in spite of an intense research, is far from being fully understood.[18] Additionally the detection and characterization of secondary relaxations taking place below the glass transition temperature (T_g), is also important since it could play a crucial role in governing crystallization, namely if it are of intermolecular nature.[19] For some ILs it was shown that the temperature dependence of the respective relaxation times behaves similarly to conventional molecular glass formers,[20] bending off while crossing T_g.[21] This feature is observed for the temperature dependence of the Johari-Goldstein (JG) process taken as the precursor of the dynamical glass transition process in the framework of Coupling Model (CM),[22] and described as the motion of the entire molecule as a whole being associated with intermolecular interactions. The assignment to a JG process will be evaluated for the tested IL-API. Finally, it is also known that water can play a role on crystallization. In aqueous sucrose mixtures the controlling step in crystallization growth is probably a dehydration mechanism, *i.e.* the migration of hydration water from the crystal surface to the bulk solution occurring prior to the incorporation of sucrose molecules in the pre-existing crystal.[23] Since [C_2OHMIM][Ibu] is highly hydrophilic, the influence of water on the conductivity and relaxation processes and on crystallization will be evaluated upon thermal cycling causing a progressive water removal of the starting moisturized material. The investigation of hydrated [C_2OHMIM][Ibu] is highly relevant since several pharmaceutics are administrated as oral liquids, intravenous infusions or, when indicated for external use, as sprays or gels, all characterized by high water contents.[24]

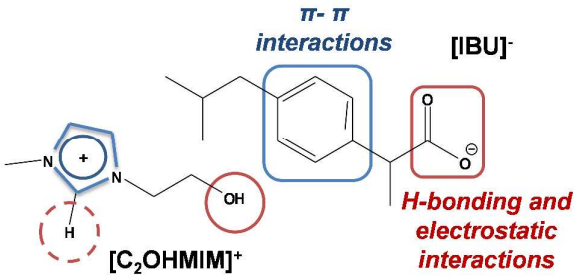

Scheme 1. Chemical structure and possible cation-anion interactions established for 1-ethanol-3-methylimidazolium Ibuprofenate, [C_2OHmim][Ibu].

Therefore, by studying [C_2OHMIM][Ibu] as a model compound, this paper addresses both practical and theoretical aspects with importance to the pharmaceutical science and industries, being a contribution to the understanding of more fundamental aspects of the condensed matter physics.

II. Experimental section

Materials

For preparing 1-ethanol-3-methylImidazolium ibuprofenate, [C_2OHmim][Ibu] (Scheme 1): 1-ethanol-3-methylimidazolium chloride (0.394 g; 2.420 mmol), was dissolved in methanol and passed through an ion-exchange column Amberlite IRA-400-OH (5 eq., flux rate 0.133 mL(mLmin)$^{-1}$). Then correspondent 1-ethanol-3-methylimidazolium hydroxide solution was slowly added to ibuprofen (0.500 g; 2.420 mmol; 1.00 eq) dissolved in methanol. The mixture was stirred at room temperature for 1 h. The solvent were then evaporated and dried under vacuum for 24h to provide the desired product as a pale yellow solid (0.7865 g; 97.76%).

^{1}H NMR (400.13 MHz, MeOD) δ 7.60 (s, 1H), 7.54 (s, 1H), 7.28 (d, J = 8.0 Hz, 2H), 7.05 (d, J = 8.0 Hz, 2H), 4.27 (t, J=4.85Hz, 2H), 3.90 (s, 3H), 3.86 (t, J=4.67Hz, 2H), 3.57 (q, J = 7.15Hz, 1H), 2.44 (d, J = 7.2 Hz, 2H), 1.83 (m, 1H), 1.42 (d, J = 7.1 Hz, 3H), 0.87 (d, J = 6.6 Hz, 6H). ^{13}C-NMR (100.62 MHz, MeOH) δ=181.86, 141.44, 138.94, 128.44, 126.95, 123.25, 122.57, 59.61, 51.82, 48.58, 44.69, 34.96, 30.11, 21.33, 18.62 ppm; FTIR (NaCl): 3361, 2957, 2218, 1906, 1565, 1459, 1388, 1287, 1169, 1071, 948, 878, 789, 654, 469 cm^{-1}. Anal. calcd for $C_{18}H_{26}N_2O_3$.3/2 H_2O C 62.59, H 8.46, N 8.11, found: C 62.25, H 8.68, N 7.86.

Solubility

The water and phosphate buffer (pH = 7.54) solubility of the novel IL-API [C_2OHmim][Ibu] was determined at 25 and 37°C showing no temperature dependence in this limited range. The maximum solubility of IL-API are presented in Table 1 and compared to the ones measured for the original ibuprofen API. For all studies the solubility profiles at 25 and 37°C were similar.

Table 1. Solubilities of [C_2OHMIM][Ibu] and Ibuprofen in water and phosphate buffer (pH = 7.54) at 25°C; values stay invariant when measured at 37°C.

	Solubility in gL^{-1} at 25°C	
compound	water	Phosphate buffer
Ibuprofen	0.021	5.9
[C_2OHMIM][Ibu]	3273	3313

Techniques

Termogravimetry Analysis

Samples of around 3 mg were placed in an open platinum sample pan and the thermogravimetric measurements were carried out with a TGA 7 apparatus from Perkin-Elmer, at a heating rate of 10°$Cmin^{-1}$ under highly pure nitrogen atmosphere with a flow rate of 20 $mLmin^{-1}$. The temperature reading was calibrated using the Curie points of alumel and nickel standards, while the mass reading was calibrated using balance tare weights provided by Perkin-Elmer. TGA analysis was used to evaluate the thermal stability of C_2OHMIM_Ibu. The obtained thermogram and the respective derivative curve (see Figure 1) show that [C_2OHMIM][Ibu] decomposes in a single weight loss step with an onset temperature of 235°C. The initial loss weight observed up to 150°C is due to water evaporation which is ca. 10% w/w for this sample.

Different samples were characterized with water contents varying between 3.5% (as freshly synthesized) and 18.8% w/w due to the hygroscopic character of the material easily absorbing water during handling under atmospheric conditions. Since the influence of water will be further discussed in more detail, a fresh sample was analyzed being submitted to two successive runs up to 150°C, revealing that it is safe to heat up to this temperature with no decomposition.

Differential Scanning Calorimetry

The calorimetric experiments were carried out with a DSC Q2000 from TA Instruments Inc. (Tzero™ DSC technology) operating in the Heat Flow T4P option. Measurements were carried out under anhydrous high purity nitrogen at flow rate of 50 $mLmin^{-1}$. DSC Tzero calibration was carried out in the temperature range from -90°C to 200°C. It requires two experiments: the first run with the empty cell (baseline) and the second run with equal weight sapphire disks on the sample and reference platforms (without pans). This procedure allows for cell resistance and capacitance calibration which compensates for subtle differences in thermal resistance and capacitance between the reference and sample platforms in the DSC sensor. Enthalpy (cell constant) and temperature calibration were based on the melting peak of indium standard (T_m = 156.60°C) supplied by TA Instruments (Lot #E10W029). Moisturized samples, with mass ~3 mg, were encapsulated in Tzero (aluminium) hermetic pans with a Tzero hermetic lid with a pinhole to allow water evaporation. To obtain the anhydrous form, the sample after a previous run from -90°C to 150°C at 10°$Cmin^{-1}$ was kept 10 min at 150°C.

To analyse in more detail the evolution of the phase transformations upon water release, a fresh moisturized sample was submitted to a thermal cycling treatment from -90°C up to increasing final temperatures, T_{end} from 60 to 150°C (ΔT_{end} = 10°C); the last cycle up to 150°C is repeated two times. The cooling rate down to -60°C was always superior to 20°$Cmin^{-1}$ being ~36°$Cmin^{-1}$ between 100 and 0°C; the heating rate was kept as 10°$Cmin^{-1}$. The overall thermal protocol is illustrated in Scheme 2.

Temperature modulated DSC (TMDSC) was also performed using different oscillation periods: 15, 20, 30, 40 and 50 s, with the respective amplitudes 0.042, 0.054, 0.08, 0.106 and 0.132 K; the heating rate was 0.5°$Cmin^{-1}$, from -60 to 15°C. At the end of each run, the sample was heated up to 150°C in order to melt any possible crystallization and the subsequent cooling was carried out at a rate of 20°$Cmin^{-1}$.

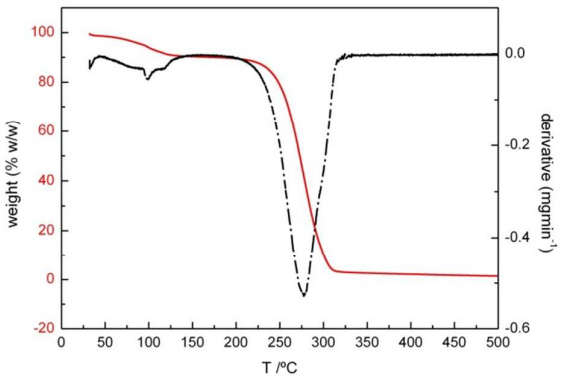

Figure 1. Thermogravimetric curve (left-hand vertical axis; black line) and derivative curve (right-hand vertical axis; red line) obtained on heating at 10°$Cmin^{-1}$ of [C_2OHmim][Ibu].

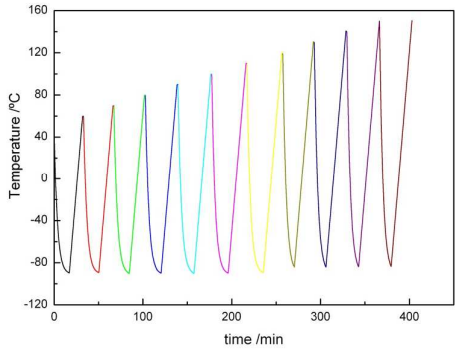

Scheme 2. DSC thermal cycling protocol used for studying water removal.

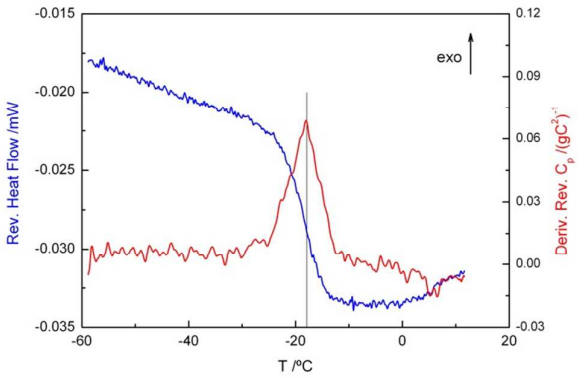

Figure 2. Thermogram obtained by TMDSC for dry [C_2OHmim][Ibu] (m = 2.77 mg) with an oscillation period of 30 s, an amplitude of 0.08°C and heating rate of 0.5°Cmin^{-1}; the line corresponding to the derivative of the heat capacity (C_p) signal was previously smoothed. The vertical line indicates the glass transition temperature extracted from modulated DSC.

An illustrative example is given in Figure 2 for an oscillation period of 30 s. The glass transition temperature was taken as the inflection point in the step change of the reversing heat flow signal which coincides with the peak seen in derivative of the reverse heat capacity.

Dielectric Relaxation Spectroscopy

Dielectric measurements were carried out using the ALPHA-N impedance analyzer from Novocontrol Technologies GmbH, covering a frequency range from 10^{-1} Hz to 1 MHz. A small amount of moisturized [C_2OHMIM][Ibu] (18.5% w/w of water content; see calorimetric section) was placed between two stainless steel electrodes of a parallel plate capacitor, BDS 1200 with two silica spacers, 50 μm thickness. The sample cell was mounted on a cryostat, BDS 1100, and exposed to a heated gas stream being evaporated from a liquid nitrogen Dewar. The temperature control is assured by the Quatro Cryosystem and performed within ±0.5 K. Novocontrol Technologies GmbH supplied all these modules. After a previous cooling ramp at 10°Cmin^{-1} from room temperature to -120°C, isothermal dielectric spectra were collected between -115°C and +150°C at different increasing temperature steps: from -100°C to -40°C in steps of 2 °C and in the remaining temperature range, every 5°C. To remove water, two fresh samples were annealed in the sample cell 30 min at 150°C, one enclosed between the two electrodes and the other in the open electrodes configuration. The latter was maintained for more 30 min at 150°C after adjustment of the upper electrode. As will be seen later on text, the first sample revealed to have ~3% w/w of water content, so from now on it will be designated as "[C_2OHmim][Ibu]$_{3\%}$", while the other it will be designated as "[C_2OHmim][Ibu]$_{anhydrous}$". Both samples were cooled down to -120°C at a cooling rate higher than 15°Cmin^{-1} to assure the avoidance of crystallization; this experimental procedure was chosen based in results obtained by DSC. Isothermal dielectric spectra were then collected between -120°C and +150°C.

Dielectric data analysis

To analyze the isothermal dielectric data, the model function introduced by Havriliak-Negami was fitted to both imaginary and real components of complex permittivity when conductivity and electrode polarization did not affect significantly the spectra. Because multiple peaks are observed in the available frequency window, a sum of HN-functions was employed:

$$\varepsilon^*(\omega) = \epsilon_\infty + \sum_j \frac{\Delta\varepsilon_j}{\left[1 + (i\omega\tau_{HN\,j})^{\alpha_{HN\,j}}\right]^{\beta_{HN\,j}}} \qquad \text{Equation 1}$$

where j is the index over which the relaxation processes are summed, $\Delta\varepsilon$ is the dielectric strength, τ_{HN} is the characteristic HN relaxation time, and α_{HN} and β_{HN} are fractional parameters ($0 < \alpha_{HN} < 1$ and $0 < \alpha_{HN}.\beta_{HN} < 1$) describing, respectively, the symmetric and asymmetric broadening of the complex dielectric function.[25]

The imaginary part of the complex electric modulus, $M(\omega)^* = M'(\omega) + iM''(\omega)$ which is widely used to suppress electrode polarization phenomena allowing revealing the dipolar contributions,[26] was analyzed through the imaginary part of Equation 1.

From the τ_{HN}, α_{HN} and β_{HN} parameters estimated from the fitting a model-independent relaxation time, $\tau_{max} = 1/(2\pi f_{max})$ was determined according to:[25]

$$\tau_{max} = \tau_{HN}\left[\frac{sin\left(\frac{\alpha_{HN}\beta_{HN}\pi}{2+2\beta_{HN}}\right)}{sin\left(\frac{\alpha_{HN}\pi}{2+2\beta_{HN}}\right)}\right]^{1/\alpha_{HN}} \qquad \text{Equation 2}$$

The non-linear temperature dependence of the relaxation times can be described by the well-known Vogel/Fulcher/Tammann/Hesse equation[27,,29] which also describes quite well the temperature dependence of dc conductivity (σ_{dc}), reading, respectively, as:

$$\tau(T) = \tau_\infty exp\left(\frac{B}{T - T_0}\right) \qquad \text{Equation 3 (a)}$$

$$\sigma_{dc}(T) = \sigma_\infty exp\left(-\frac{B_\sigma}{T - T_{0,\sigma}}\right) \qquad \text{Equation 3 (b)}$$

where τ_∞ and σ_∞ are the values of the relaxation time and conductivity in the high temperature limit, B (or B_σ) is an empirical parameter characteristic of the material accounting for the deviation of linearity (roughly the lower B the more curved is the 1/T plot) and T_0 ($T_{0,\sigma}$) is the Vogel temperature, that can be related, for the equation expressed in relaxation time (Equation 3a), to the glass transition temperature of an ideal glass, *i.e.*, a glass obtained with an infinitely low cooling rate.[30] σ_{dc} in Equation 3b is obtained by simulating the real conductivity frequency dependence by the equation proposed by Jonscher[31]:

$$\sigma'(\omega) = \sigma_{dc}\left[1 + \left(\frac{\omega}{\omega_{cross}}\right)^s\right] \qquad \text{Equation 4}$$

where s ($0.5 \le s \le 1$)[12] is a material and temperature dependent parameter and ω_{cross} is the onset of the ac conductivity.

Polarized Optical Microscopy

Polarized optical microscopy was performed on an Olympus Bx51 optical microscope equipped with a Linkam LTS360 liquid nitrogen-cooled cryostage. The microstructure of the samples was monitored by taking microphotographs at appropriate temperatures, using an Olympus C5060 wide zoom camera. A sample of moisturized [C_2OHmim][Ibu], was positioned on a microscope slide and inserted in the hot stage. To monitor the emergence of crystallization, the sample was previously submitted to the same thermal treatment followed in DSC experiments by heating at 150°C and maintaining 10 minutes at this temperature before putting a cover slip; then it was submitted to a cooling ramp at 20°Cmin^{-1} down to -90°C. Microphotographs were taken in the subsequent heating run at 10°Cmin^{-1}.

III. Results

Calorimetric and optical results

Due to the high hydrophilicity of [C_2OHmim][Ibu], samples with different moisture levels were submitted to a first heating run from -90 to 150°C at 10°Cmin^{-1}, being kept 10 min at 150°C in order to eliminate water. Besides the broad endotherm peak centered at around 96°C due to the water evaporation, a clear signal of the glass transition can be observed at low temperatures (see blue and black solid lines in Figure 3a), with a location that highly depends on the water content (estimated from the weight loss of each sample). For samples with 18.5% w/w and 15% w/w of water content, the glass transition temperature measured in the onset ($T_{g\text{-}on}$) was, respectively, -76.9°C and -70.9°C; the moisturized sample with 18.5% w/w of water content was divided in two aliquots for DSC and DRS measurements. For the anhydrous state (red curve), the glass transition temperature significantly shifts to higher temperatures being $T_{g\text{-}on,anhydrous}$= -21.3 °C irrespective to the initial water content. This represents an increase of around 50°C relative to the glass transition temperature of samples with water contents above 14.4% ($T_{g\text{-}on}$ = -70.3°C; see Figure 5). This strong deviation of the temperature location of the glass transition is of the same order as observed for water mixtures of the ionic liquid lidocaine HCl vs anhydrous lidocaine HCl[24] but considerably higher to which is usually found for ILs[32,33,34] and ILs based materials.[21] The significant shift in the glass transition upon hydration may indicate a structural effect due to water incorporation that would lead to breaking of extended anion-cation interactions.

The heat capacity change at the glass transition for anhydrous C_2OHmim_Ibu was estimated as ΔC_p = 0.45 J(gK)$^{-1}$, after correction taking in account the sample loss mass due to water evaporation; the value for the 14.4% w/w sample was ΔC_p = 0.63 J(g°C)$^{-1}$.

Additionally, the thermogram for the dried sample (red curve in Figure 3a) shows two exothermic peaks indicating crystallization whose maxima are located at 39.7 and 71.5°C. At higher temperatures, a bimodal endothermic peak is clearly detected with two minima at 107 and 114°C due the melting of the previously crystalline structure formed.

For the samples whose thermograms are included in Figure 3a, crystallization was avoided in the cooling scan after annealing at 150°C. To evaluate the influence of the cooling rate in the emergence of melt crystallization, different scans carried out at cooling rates between 20 and 3°Cmin^{-1} were performed for a sample dried 10 min at 150°C, showing that melt crystallization is avoided if the cooling rate is kept >10°Cmin^{-1} (not shown). For cooling rates of 10, 5 and 3°Cmin^{-1}, melt crystallization is always observed between 20 and 40°C (see exothermal in the inset of Figure 3b for the ramp carried at a cooling rate of 3°Cmin^{-1}), however in the subsequent up scans (main Figure 3b) the glass transition step and cold crystallization are still detected, in the same temperature regions as occur for the initially full amorphous dried sample (red line in Figure 3a).

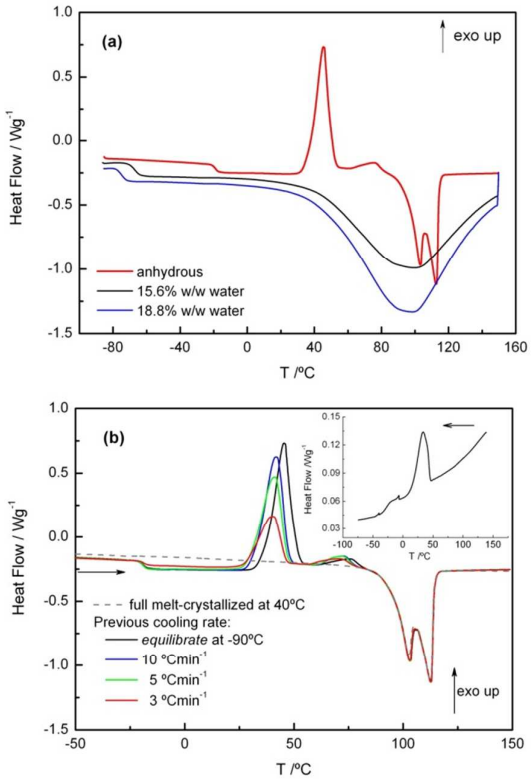

Figure 3. a) Heat flow thermograms for samples with different water contents (see legend) obtained upon heating at 10°Cmin^{-1} before (blue and black solid lines) and after (red curve) being kept 10 min at 150°C; the cooling rate between 1st and 2nd heating runs was higher than 20°Cmin^{-1} (see *Experimental*). b) Heat flow thermograms for samples with different crystallinities induced in the previous cooling ramp at the indicated rates and the up scan of a sample full melt-crystallized (1 hour at 40°C) evidencing the invariance in the two peaks profile of melting; the down scan of a cooling ramp carried at 30°Cmin^{-1} is included in the inset to illustrate melt-crystallization.

This shows that the material is semi-crystalline at the end of the previous cooling scan and that the glass transition and type of cold crystallization are not affected by the achieved crystallinity degree, only the extension of both phenomena.

Indeed, the bimodal nature in both crystallization and melting events is always observed upon heating in thermograms collected for either initially amorphous or (semi) crystalline dried samples and may be originated by the emergence and fusion of different crystalline structures. To investigate this in more detail, two different assays consisting in the isothermal crystallization from the melt (sample cooled down from 150°C at 20°Cmin^{-1}) at 40 and 20°C were conducted and monitored by polarized optical microscopy (POM).

Microphotographs obtained at the end of crystallization are present in Figure 4: the one obtained at T_{crys} = 40°C appears as a sandy texture while for crystallization at T_{crys} = 20°C, well defined spherulites emerge. In both cases, full melting is observed on crossing 110°C in good agreement with the DSC results. When the spherulitic morphology is obtained, it seems to convert to the sandy texture above 90°C which could correspond to the first endothermic transition detected in the thermograms.

The possibility of the ibuprofenate anion to interact with the C_2OHMIM cation via H-bonds through either the hydrogen from the OH group or the proton marked by a dashed red circle in Scheme 1 of the imidazolium unit, could be in the origin of distinct crystalline forms in [C_2OHmim][Ibu]. Further investigation must be done in order to clarify this aspect, requiring X-ray diffraction studies to analyze if two different crystalline structures or different crystalline sizes are being observed. Additionally, the two endothermic peaks attributed to melting could also involve a kind of solid-solid transition. Studies to clarify this subject, including the dynamic behavior of the crystalline structure that seems to be compatible with a plastic crystalline phase are ongoing.

Aiming to study in more detail the evolution of phase transformations with the water release, successive cooling and heating runs according the thermal cycling treatment schematized in the *Experimental* section (see Scheme 2) were conducted in a fresh moisturized sample (14.4% w/w water). The obtained thermograms are plotted in Figure 5 from which several features can be observed: i) at the lowest temperatures, a systematic deviation of the glass transition towards higher temperatures occurs, varying from -70.3°C (1st run) to -21.6°C, the latter being detected in the up scan taken after the cycle ending at 130°C remaining unchanged upon further increasing of T_{end}; ii) in the temperature range between ~15 and ~70°C, two exothermic peaks emerge due to cold crystallization for runs subsequent to the one ending at 90°C; iii) cooling at this relatively high rate (>20°Cmin^{-1}) occurs without melt crystallization except for the cooling scans taken after 100 and 110°C, leading to the vanishing of the glass transition step and of the exothermical peaks due to cold-crystallization in the immediately successive up scans; additionally iv) either bulk water crystallization or melting (seen as a sharp peak at 0°C)[34] are absent in the thermograms; this observation and the detection of only one glass transition seems to indicate a strong binding of water in the structure of the ionic liquid as noted by others for a IL[33] turning this salt highly water soluble.

Values of the glass transition temperatures measured in the onset ($T_{g\text{-}on}$), peak temperatures of crystallization and melting are included in Table 2. In the inset of Figure 5 the T_g dependence with the water content is plotted for a set of [C_2OHmim][Ibu] samples calorimetrically characterized having hydration levels between 7.5 and 18.8%. A simulated data point (filled circle) is included in the figure corresponding to a T_g = -30°C. From the polynomial fit a water content of 2.6% w/w is estimated and therefore this sample is designated "[C_2OHmim][Ibu]$_{3\%}$". The T_g value was assumed to be

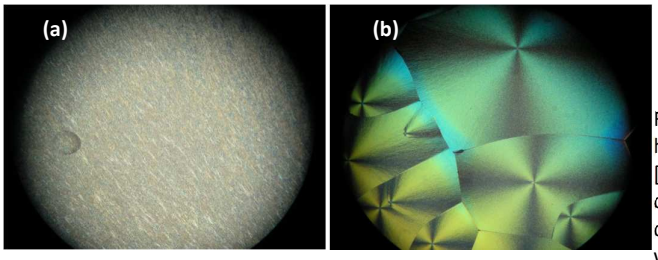

Figure 4. Microphotograhs taken with cross-polarizers and magnification of 40x of dried samples isothermally melt-crystallized: (a) during 60 min at 40°C and (b) during 30 min at 20°C. The liquid (dried) [C_2OHmim][Ibu] was cooled down to the crystallization temperatures at 20°Cmin^{-1}.

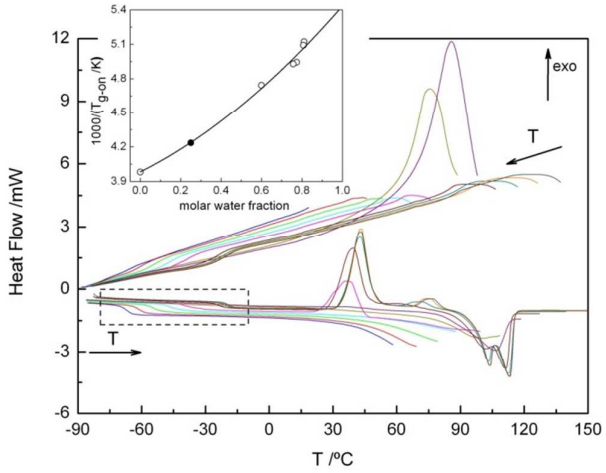

Figure 5. Heat flow thermograms obtained upon cooling and heating at a rate of 20°Cmin^{-1} for an initially moisturized [C_2OHmim][Ibu] (14% w/w water) sample submitted to the thermal cycling treatment depicted in Scheme 2 (see *Experimental*); the dashed rectangle indicates the evolution of the glass transition with water removal. In the inset the plot of the reciprocal of $T_{g\text{-}on}$ *vs* molar fraction of water is included for samples with different hydration levels; the solid line is the polynomial fit. The filled point corresponds to an estimate value of the water content for a T_g = -37°C (see text).

the glass transition temperature of the sample annealed at 150°C and dielectrically characterized (see next section). At the end of this section it is important to summarize the main observations resulting from calorimetric measurements: [C_2OHmim][Ibu] is miscible with water retaining contents up to 19% w/w when let it to equilibrated with moisture under atmospheric conditions; the glass transition temperature of the aqueous mixture is highly shifted (~50°C) to lower temperatures relative to the anhydrous state, due to the plasticizing effect of water, as already observed by some of us for dicyanamide-based ionic liquids.[21,32]

The water evaporation profile as registered in the thermogram presented in Figure 3a, shows that the emerging of crystallization is observed only after the cycle ending at 90°C, meaning that a significant amount of water must be removed to allow crystal growth in [C_2OHmim][Ibu]. This is coherent with the findings reported in reference 23 (see also *Introduction*) where it is admitted that crystallization growth is controlled by a de-solvation step with transference of hydration water from the crystal surface to bulk solution. From the condition at which melting of the crystalline structure formed upon cold crystallization is observed by the first time, the profile and location of the correspondent endothermic event is kept unchanged irrespective to the water content. This means that the water molecules that subsist do not interfere with the crystalline structure, only influence the crystalline fraction formed.

Table 2. Temperatures of the thermal events for [C_2OHmim][Ibu] with 14.4% w/w of water content according the thermal treatment of Scheme 2, whose thermograms are presented in Figure 5.The first column indicates the final temperature of each run. Glass transition temperatures were measured in the onset ($T_{g\text{-}on}$) and midpoint ($T_{g\text{-}mid}$), crystallization and melting temperatures correspond to the maximum and minimum of the respective peaks (T_{max}, T_{min}).

Run	Glass transition		Cold-crystallization		Melting	
T_{end} (°C)	$T_{g\text{-}on}$ (°C)	$T_{g\text{-}mid}$ (°C)	$T_{max\text{-}1}$ (°C)	$T_{max\text{-}2}$ (°C)	$T_{min\text{-}1}$ (°C)	$T_{min\text{-}2}$ (°C)
60	-70.3	-67.3				
70	-65.4	-61.0				
80	-58.1	-54.4				
90	-50.6	-47.2				
100	-43.2	-39.8	36.8			
110	*	*				
120	*	*			106.0	
130	-26.1	-23.8	39.7	61.7		111.0
140	-22.8	-20.1	42.5	71.4	102.8	112.4
150	-21.8	-19.3	42.9	75.7	103.5	112.8
150	-21.6	-18.9	42.9	76.9	103.8	113.0

(*) Ill-defined glass transition region due to the occurrence of crystallization on cooling (melt-crystallization).

Moreover, the reproducibility of the two peaks profile upon melting in samples undergoing melt and/or cold crystallization, isothermally or non-isothermally crystallized mean that the same crystalline structure is built in (semi) crystalline [C_2OHmim][Ibu].

Dielectric results

An aliquot of the same moisturized sample (18.5% w/w) previous analyzed by DSC was studied by DRS; hereafter this sample will be designated [C_2OHmim][Ibu]$_{18.5\%}$. The sample was directly cooled down to -120°C from room temperature and then submitted to isothermal measurements upon heating (see *Experimental*). Since data are highly influenced by conductivity and electrode polarization above ~ -78°C, it is convenient to analyze the dielectric response through the complex electric modulus (M*) (see *Introduction*). The respective imaginary part is represented in Figure 6a between -115 and -60°C. At the lowest temperatures, in the glassy state, a rather intense secondary β-process is detected. This process is also observed in the ε´´ representation, revealing that reorientational dipolar motions are in its origin. Its intensity is highly enhanced by the incoming of another relaxation process, suggesting a close coupling between both processes. This latter process is not unambiguously seen in ε´´ spectra being masked by the high conductivity. It should be noted that for another ionic liquid butyl-methyl-pyridinium dicyanamide, [BMPyr][DCA],[21] two well resolved and intense processes were detected above T_g in the modulus formalism: one process associated with the dynamic glass transition (α-process) and another, at higher temperatures and lower frequencies, associated with conductivity (σ-process). Contrary to [BMPyr][DCA], for [C_2OHmim][Ibu]$_{18.5\%}$ no such two processes were detected even at temperatures as high as 150°C. Therefore, this dominant process has the contribution of both α and σ processes, and will be named σα-process as adopted in reference [35].

The above results for [C_2OHmim][Ibu]$_{18.5\%}$ will be now compared with the ones found for samples measured after annealing at 150°C: [C_2OHmim][Ibu]$_{3\%}$ and [C_2OHmim][Ibu]$_{anhydrous}$ (see *Experimental*).

The ε´(T) traces at 10^4 Hz upon cooling at ~15°Cmin^{-1} for the three samples are plotted in Figure 7. The first observation is the significant shift to higher temperatures with water removal of the region where dipolar response associated with the dynamical glass transition is detected. This is coherent with the deviation of the glass transition region as observed by DSC with the progressive drying.

Moreover, for [C_2OHmim][Ibu]$_{3\%}$ and [C_2OHmim][Ibu]$_{anhydrous}$ (green and red symbols) no signs of discontinuity in ε´(T) is detected in the temperature region where melt-crystallization was observed by DSC (inset in Figure 3b), indicating that full amorphous materials are obtained after this thermal treatment. Contrary, on heating from the glass, the ε´(T) traces at 10^4 Hz (taken from isothermal measurements) show a discontinuity between 32°C and 89°C for the 3% sample (not shown) and from 10 to around 110°C for the anhydrous one (white

triangles); in both cases there is a reasonable agreement with the calorimetric observations. Therefore cold-crystallization and further melting are also observed by DRS measurements.

The isothermal M´´ spectra collected for $[C_2OHmim][Ibu]_{3\%}$ and $[C_2OHmim][Ibu]_{anhydrous}$ are presented in Figure 6b and Figure 6c, respectively. From -120 to -60°C for $[C_2OHmim][Ibu]_{3\%}$, two relaxation processes are distinguished (named β and γ) also observed in the ε´´ representation confirming its dipolar nature. At higher temperatures, a third peak (σα) is visible dominating the spectra above -40°C. For the anhydrous one, two processes are clearly observed, one at the lowest temperatures with more or less the same location than the γ-process of $[C_2OHmim][Ibu]_{3\%}$; the other one (σα) is visible above -22°C. For both samples the dominating process can be assigned to the homologous σα-process found in the $[C_2OHmim][Ibu]$ with 18.5% water content. It is noteworthy that in anhydrous $[C_2OHmim][Ibu]$ the β-process which is hardly visible in the M´´ isotherms it can be clearly observed in the isochronal M´´(T) representation (inset of Figure 7).

The M´´ spectra and ε´´ spectra (when the contribution of conductivity is low) were analyzed to extract the relaxation times (see *Experimental*), which were converted to τ_{max} by Equation 2. The thus obtained relaxation times are plotted in Figure 8, for the 18.5%, 3% and anhydrous $[C_2OHmim][Ibu]$. Shape parameters of the process detected are summarized in Table 3.

From the relaxation map (Figure 8) several features must be pointed out that will be summarized in the next lines. The first observation is the significant shift towards higher temperatures of the relaxation times estimated for the processes detected for the anhydrous sample relatively to the moisturized ones, confirming the plasticizing effect of water observed by DSC. Secondly, in the sub-T_g region the relaxation times (log τ vs. 1/T) of the secondary processes obey to an Arrhenius temperature dependence, $\tau(T) = \tau_\infty exp(E_a/RT)$, being linear in the relaxation map. It is important to note that the dielectric response below T_g is of dipolar nature where the ionic species behave mostly as a single ionic dipole. In this context, a very localized mechanism must be in the origin of the γ-process detected in the anhydrous and 3% samples due to: i) it is active at extremely low temperatures compared with the calorimetric glass transition temperature; ii) the low activation energy estimated from Arrhenius law (22.4 kJmol^{-1}; see Table 3); iii) the pre-exponential τ_∞ factor, that it is of the order of 10^{-12} s as the typical values for non-cooperative Debye process originated by local orientational fluctuations (10^{-12}–10^{-14} s).[36]

Concerning the temperature dependence of relaxation times of the secondary β-relaxation, its trace changes to a higher activation energy regime after crossing a temperature near T_g. The bending of the β-trace is observed for the temperature dependence of the Johari-Goldstein (JG) process taken as the precursor of the relaxation process responsible for the dynamical glass transition in the framework of Coupling Model (CM).[22] This type of behavior has been observed in many glass formers including ionic liquids.[20,21,35]

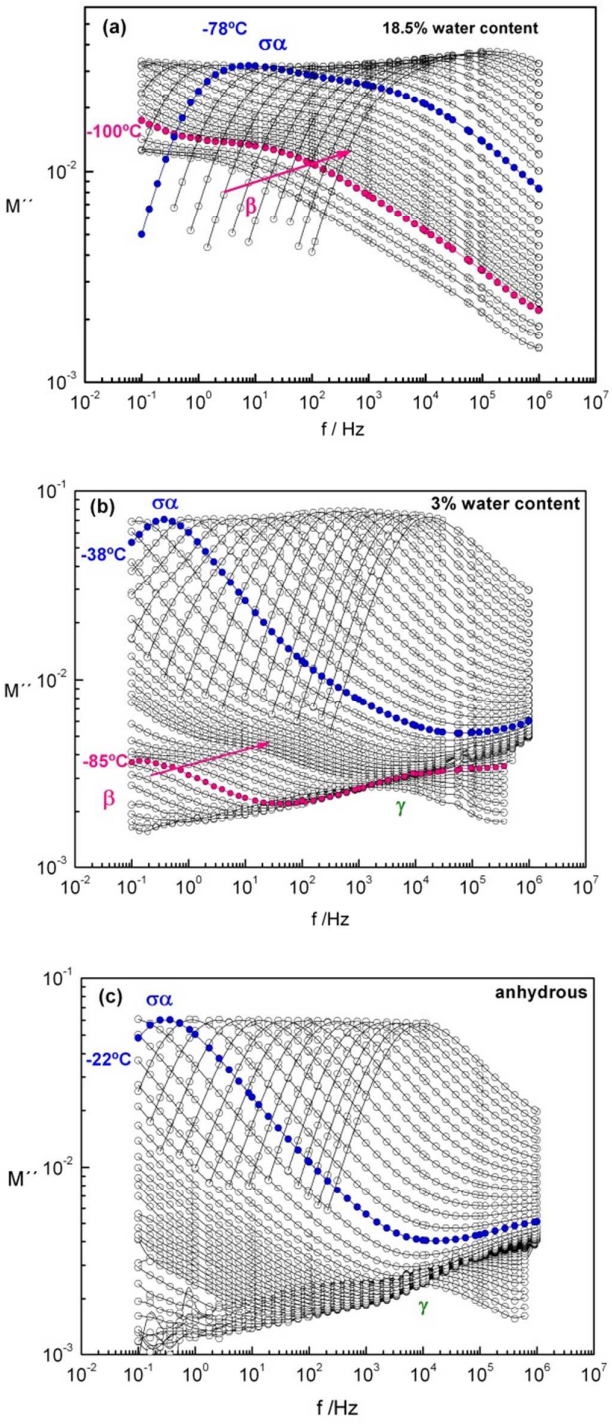

Figure 6. Isothermal spectra of the imaginary part of the complex modulus of: (a) $[C_2OHmim][Ibu]_{18.5\%}$, for temperatures from -115 to -60ºC (from -115 to -100 every 5°C, and from -98 to -60°C every 2 degrees); (b) for $[C_2OHmim][Ibu]_{3\%}$, between -135 and -6°C (from -135 to -60°C the spectra are represented every 5ºC and from -58 and 0°C, every 2°C); (c) $[C_2OHmim][Ibu]$ anhydrous, for temperatures from -100 to 6°C (from -100 to -60 every 5°C, and from -38 to 6°C every 2 degrees).

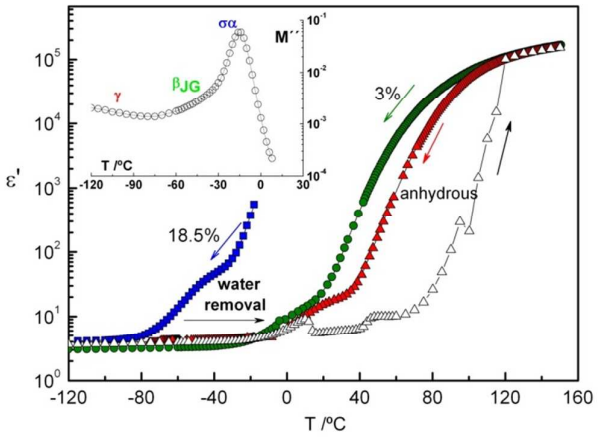

Figure 7. Isochronal ε´(T) plot at 10^4 Hz for [C_2OHmim][Ibu] with different water contents collected during cooling scans at ~15°Cmin^{-1} (colored filled symbols); also ε´(T) taken from isothermal data collected on heating for anhydrous [C_2OHmim][Ibu] is included (white triangles). In the inset is represented the isochronal plot of M´´ at f = 10 Hz where three processes are visible.

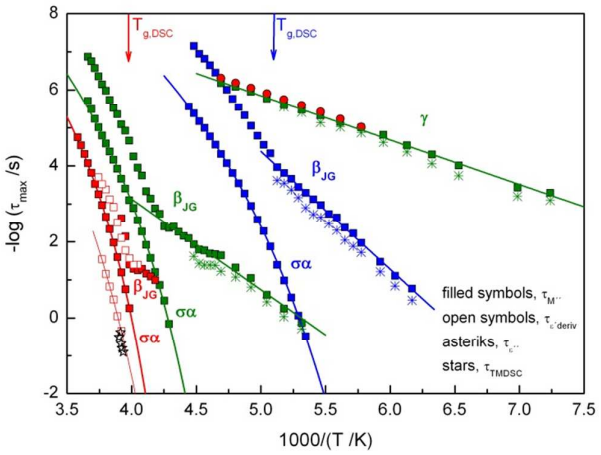

Figure 8. Relaxation map of all detected processes for amorphous [C_2OHmim][Ibu] extracted from M´´ for: 18.5% (blue symbols), 3% (green symbols) and anhydrous sample (red symbols); the relaxation times estimated from the analysis of ε´´ are included as asterisks. The open red squares are the relaxation times obtained from the ε''_{deriv} for anhydrous [C_2OHmim][Ibu]. The solid lines are the Arrhenius and VFTH fitted curves for secondary and σα processes. Arrows indicate the reciprocal of the calorimetric glass transition temperature ($T_{g\text{-}on}$) for [C_2OHmim][Ibu] 18.5% w/w and anhydrous (standard DSC measurements). Black stars are the structural relaxation times estimated from TMDSC measurements.

For [C_2OHmim][Ibu]$_{18.5\%}$ the bending of the β-trace occurs at -76°C in very good agreement with the DSC glass transition temperature (-76.9°C). Assuming that this behavior is also obeyed by the [C_2OHmim][Ibu]$_{3\%}$ sample, a value of -37°C is estimated for T_g from the bending of the $\beta_{3\%}$-trace. This T_g value was used in the plot of the reciprocal of the respective glass transition temperatures *vs.* water molar fraction presented in the inset of Figure 5, allowing to estimate a water percentage of ~3% for the sample submitted to an annealing at 150°C for 30 minutes in closed electrode configuration (see *Experimental*).

It is important to note that, in spite of this intense thermal treatment, the sample still retains water indicating how strong it is the interaction between the ionic liquid and water molecules. This "residual" water must be differentiated from simple physically adsorbed water that is easily removed below 150°C, as concluded from the TGA analysis, having a high impact in the thermal and dielectric properties of the material. In this context, the presence of water manifests in the β-relaxation, whose intensity is enhanced from anhydrous to 3% due to the high dipole moment of the water molecules coupled with the active dipole of [C_2OHmim][Ibu] that it is relaxing. This effect is even more pronounced when the more mobile adsorbed water is present, as for [C_2OHmim][Ibu]$_{18.5\%}$ for which the β relaxation becomes more resolved from the σα-process. This seems also to affect the energy barrier that must be overcome in the reorientational motion behind this process in the sub-T_g region. Since both the water molecules and ionic liquid have the ability to interact *via* hydrogen bonds, this may be the reason why the activation energy increases (see $E_a(\beta)$ values in Table 3) as observed for molecular glass formers- water mixtures (37 and references therein). The estimated activation energy values can be used to confirm if the observed relaxation is a JG process.

Kudlik *et al* [38] proposed that its activation energy should obey to the ratio $E_{a,\beta}/RT_g \approx 24$ ($E_{a,\beta}$ is the glassy state activation energy of the β_{JG}-process, T_g is the dielectric glass transition temperature taken for τ_α = 100 s, and R is the universal gas constant). For the 3% sample a good accordance is obtained since values of 22 and 23 are estimated by considering the activation energy derived from, respectively, log$\tau_{\varepsilon''}$ *vs* log*f* and log$\tau_{M''}$ *vs* log*f*; T_g was replaced by the temperature at which the β-trace bends off (-37°C). For the 18.5% sample a much higher value is obtained, 37. Although values close to 24 are found for several glass formers, there are some exceptions to this correlation,[39] which could be the case for the moisturized material. Nevertheless, it is worthwhile to analyze the pre-exponential factor of this process in the sub-T_g region for both tested samples. While for the 3% one, a value close to Debye time, ~10^{-12} s (log$\tau_{\varepsilon''}$) and ~10^{-13} s (log$\tau_{M''}$) was estimated, for the 18.5% sample the pre-exponential factor is ~10^{-20} s. This could indicate some complexity of this process probably due to the above mentioned coupling with reorientational motions of water molecules involving hydrogen bonding exchange. Additionally, the abnormally low pre-exponential factor may be originated by a distribution of activation energies as discussed in reference[40] for maltitol and other glass formers by comparing DRS and thermal stimulated depolarization currents (TSDC) data. While DRS gives an activation energy of 57 kJmol^{-1} and τ_0 ~ 10^{-16} s for maltitol, TSDC gives an energy distribution width of 30 kJmol^{-1} (39 - 70 kJmol^{-1}) and τ_0 ~ 10^{-13} s. Therefore the hypothesis of a JG process is still considered for the 18.5% sample reinforced by the observation of

the bending of the β-trace at the calorimetric glass transition temperature.

It is important to note that the JG process is intermolecular in nature and thus may have a role in controlling crystallization.[19] This process is observed for the three systems here studied (although ill-defined due to M´´ dominant σα-process in the anhydrous [C_2OHmim][Ibu]). While in anhydrous and [C_2OHmim][Ibu]$_{3\%}$ the β-JG process can be an important contribution for the observed cold-crystallization near above T_g, in the 18.5% moisturized sample, crystal growth is inhibited probably due to the high ratio of water molecules impair the [C_2OHmim][Ibu] salt to organize and/or incorporate in a crystalline structure as suggested for sucrose.[23]

In the relaxation map, the trace of the σα-process is curved for the three samples [C_2OHmim][Ibu] and the respective temperature dependence of relaxation times obeys to a VFTH (Equation 3a); the corresponding parameters are presented in Table 3. This kind of curvature suggests that structural relaxation*, i.e*. the molecular motions that govern transport properties determining the dynamic glass transition, contributes to the temperature dependence of the σα-process. The dielectric loss spectra, ε"(ω), of dipolar glass-formers are dominated by this structural process associated with reorientational motions of dipoles. In glass forming ionic conductors as [C_2OHmim][Ibu], the high contribution of conductivity impairs the direct access to this process.

To overcome such difficulty, the real permittivity spectra can be analyzed through its derivative that eliminates the dc conductivity contribution, which strongly affects ε´´(ω) data ($\varepsilon''_{deriv} \approx -\frac{\pi}{2}\frac{\partial\varepsilon'(\omega)}{\partial ln\omega}$).[41] This procedure was applied to the ε´(ω) spectra of the anhydrous sample near above the glass transition temperature letting to distinguish two processes of dipolar origin: the α-relaxation and the β-JG relaxation (this analysis was not done for 18.5% sample due to the strong influence of electrode polarization). The HN function was fitted to the ε''_{deriv} loss curves allowing extracting the respective relaxation times which are included in the relaxation map shown in Figure 8 (open red squares). To confirm the assignment of the α-relaxation, temperature modulated DSC experiments were carried out. The correspondent calorimetric structural relaxation times were estimated from the temperature dependences of the reverse of both heat flux and heat capacity signals (see Figure 2), and are plotted in the relaxation map (stars) revealing excellent agreement with $\tau_{\varepsilon''deriv}$. This strongly supports the previous assignment that besides conductivity also dipolar reorientations contribute to the σα-process observed in the M´´ spectra.

To have now an insight in the conductivity contribution, in the next section the conductivity spectra will be analyzed.

Conductivity analysis

Spectra of σ´(f) of 18.5% w/w water content and anhydrous [C_2OHmim][Ibu] are characterized by a plateau in the low frequency side corresponding to the direct current (σ_{dc}) due to the motion of free charge carriers, and a transition to a frequency dependence behavior characteristic of a.c. conductivity; the latter corresponds to semi-diffusive hopping conduction at short-range distance in the material. This behavior is exemplified for sample with 18.5% w/w of

Table 3. Fitting parameters for [C_2OHmim][Ibu] obtained for M´´ and ε´´ analysis of dielectric spectra.

	process	Temperature range (ºC)	-log(τ_0 /s)	B (K)	T_0 (K)	E_a (kJmol^{-1})	E_a/RT_g	α_{HN} β_{HN}
Modulus (M´´)								
18.5%	σα	[-86,-48]	13.3±0.2	1537±62	138±1			0.50→0.90 0.41±0.07
	β	[-111,-60]*	19.9±0.2			59.2	37	0.35→0.62 0.55→0.31
3%	σα	[-40,0]	15.7±0.7	2580±274	162±5			0.8±0.04 0.98±0.02
	β	[-85,-38]*	12.6±0.3			45.6	23	0.76→0.49 0.66±0.07
	γ	[-135,-60]	11.7±0.1			22.4		0.31±0.04 0.68±0.01
anhydrous	σα	[-22,6]	12.2±0.6	1299±168	203±4			0.71→0.91 1→0.36
Permittivity (ε´´)								
18.5%	β	[-111,-78]*	19.3±0.2			58.4	37	0.35→0.45 0.70±0.02
3%	β	[-85,-50]*	11.6±0.5			42.7	22	0.43±0.02 1
	γ	[-135,-80]	12.0±0.2			24.0		0.25±0.01 1

* Values obtained for the temperature region below the corresponding T_g.

water in Figure 9. Using the so called 'Summerfield scaling'[42] the σ´ spectra were normalized (representation of $\log(\sigma'/\sigma_{dc})$ *vs.* $\log(f(\sigma_{dc}T)^{-1})$ in the inset of Figure 9 for the 18.5% w/w sample). The master curve obtained indicates the temperature independence of the curve shape, which means that the subjacent conductivity mechanism is the same in all temperature range analyzed. Electrode polarization due to space charge accumulation at the sample/electrode interface is also observed at higher temperatures by a decrease in the low frequency side of σ´ spectra.

Jonscher's equation (Equation 4) has been used to fit σ´ spectra in the frequency range in which σ´ is not influenced by electrode polarization. The temperature dependence of σ_{dc} that is commonly associated to long-range movement of free charge carriers is plotted in Figure 10. As it could be expected, the water in these samples facilitates this type of movements by decreasing viscosity and weakening the contact between ion-pairs by displacing the heavier counterions from the respective coordination shells, which reduces caging and increases the diffusivity[43]. This leads to higher values of dc conductivity (at the same temperature). A clear departure of the Arrhenius behavior of $\log(\sigma_{dc})$ *vs.* 1/T is observed being well described by the empirical VFTH equation. The obtained VFTH fitting parameters for 18.5%, 3% and anhydrous samples are summarized in Table 4. This curvature described by $\log(\sigma_{dc})$ *vs.* 1/T has been observed in many glass-formers for the relaxation time of the main process associated to the dynamic glass transition. The similarity suggests a correlation between the dynamics of the structural relaxation and the ion motions responsible for the dc conductivity, σ_{dc}. From this property it is possible to estimate the relaxation time for dc conductivity, τ_σ, according to $\tau_\sigma = \varepsilon_\infty \varepsilon_0 / \sigma_{dc}$ [44]. Figure 10b shows a simplified relaxation map where τ_σ(T) for the 18.5% w/w water and anhydrous [C_2OHmim][Ibu] samples are compared with the respective relaxation times obtained for the main process detected in the modulus formalism ($\tau_{\sigma\alpha}$(M´´)) and for the α-relaxation, $\tau_\alpha(\varepsilon''_{deriv})$.

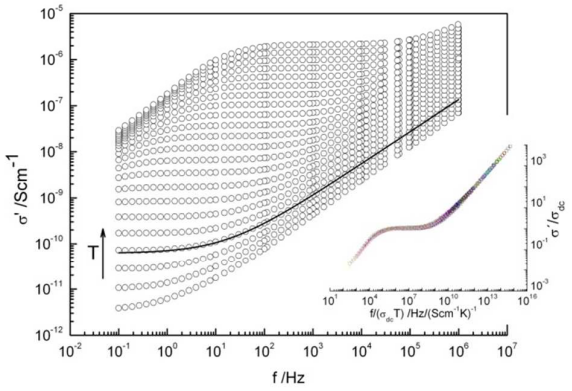

Figure 9. Real conductivity spectra of [C_2OHmim][Ibu] with 18.5% w/w of water taken from -78 to -38°C every 2 degrees. The solid line is the obtained fit by the Jonscher´s law (Equation 4) to the σ´(f) data taken at -74°C as example. In the inset are represented the normalized spectra for the same temperatures.

Table 4. VFTH parameters of $\log(\sigma_{dc})$ *vs.* 1/T, value of σ_{dc} at calorimetric $T_{g\text{-}on}$ = -76.9°C and -21.3°C for 18.5% and anhydrous sample; the temperature range refers to the interval within which the Jonscher's equation was used. The σ_{dc} for the 3% sample is not given due to the lack of its calorimetric T_g.

	Conductivity (σ_{dc})				
sample	Temperature range (°C)	$\log(\sigma_0$ /Scm$^{-1})$	B (K)	T_0 (K)	$\sigma_{dc}(T_{g,DSC})$ (Scm^{-1})
18.5%	[-78,38]	2.3 ± 0.1	1860 ± 18	134.5 ± 0.8	1.7×10^{-11}
3%	[-30,0]	1.2 ± 0.9	1571 ± 289	188 ± 6	.....
Anhydrous	[-14,8]	-1.9 ± 0.3	742 ± 67	223 ± 2	5.5×10^{-14}

The τ_σ(1/T) and $\tau_{\sigma\alpha}$(M´´)(1/T) traces overlay at high temperatures for both moisturized and anhydrous materials indicating a dominance of conductivity in the dielectric response well above the glass transition. In the vicinity of T_g, τ_σ of the dried sample differentiates from $\tau_{\sigma\alpha}$(M´´) going closer to $\tau_\alpha(\varepsilon''_{deriv})$ driven by the dynamics of the glass transition. This leads to conclude for a strong coupling between conductivity and structural relaxation, suggesting a dynamical glass transition assisted hopping mechanism as reported for other ionic liquids.[45] Additionally, it is worth to note that the modulus still exhibits a peak when the conductivity doesn't exhibit a dc plateau. For the hydrated sample it is extended deeply below the glass transition, i.e., when the ionic liquid matrix is vitrified and therefore the long distance translational motion of charge carriers is frozen. This seems to point to a subjacent conduction mechanism originated mainly by short-range motions of water ions that persist below T_g, being essentially sub-diffusive. [46]

The dynamical profile of the structural relaxation and conductivity process close to T_g for [C_2OHmim][Ibu], is similar to the one exhibited by a protic ionic liquid[35] and different to which is observed for an aprotic one, $[BMPyr][DCA]_{30\%}$.[21] In fact, the relative location in the relaxation map of τ_α and τ_σ is unexpected for an aprotic IL as [C_2OHmim][Ibu] which doesn't allow free protons motion that originates a faster conduction. The rationalization of the observed behavior for [C_2OHmim][Ibu] can be made based on the expected multiplicity of cation-anion interactions as depicted in Scheme 1. Contrary to aprotic ILs for which the cation and anion interact only electrostatically, forming a charge compensated ion pair, in [C_2OHmim][Ibu] also H-bonding and π-π interactions can be possible. Since these may manifest with different extensions, a complex overall behavior is expected including reorientational motion (as occurs for a conventional glass former) and migration of uncompensated charge species.

The richness of possible interactions will favor the interaction with water molecules originating a much more soluble material comparing to the original molecular drug that only interacts via H-bonding. Indeed, the solubility in water for

[C_2OHmim][Ibu] is increased around 5 orders of magnitude compared to the one of molecular ibuprofen (see Table 1).

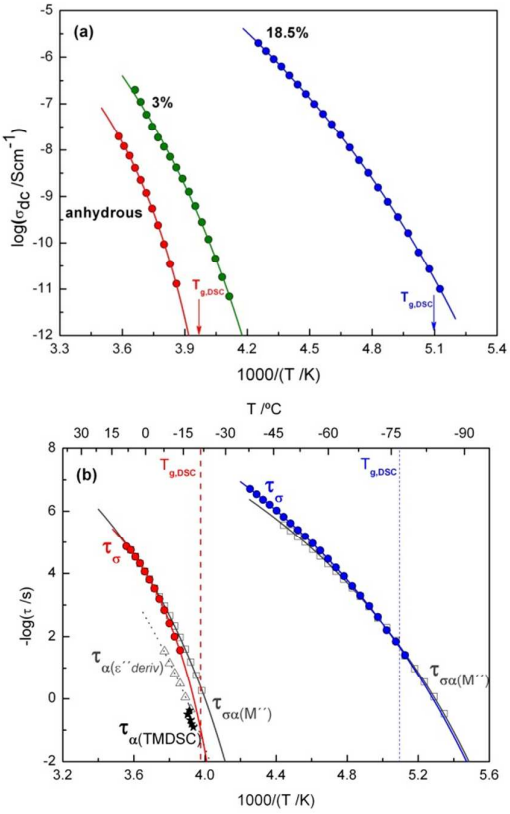

Figure 10. (a) Temperature dependence of the dc conductivity obtained from the Jonscher's equation for 18.5%, 3% and anhydrous [C_2OHmim][Ibu]. Lines are the fitted VFTH curves (Equation 3b). The arrows indicate the calorimetric glass transition temperatures for anhydrous and 18.5% samples. (b) Simplified relaxation map for 18.5% and anhydrous [C_2OHmim][Ibu] including relaxation times obtained from: M´´ spectra ($\tau_{\sigma\alpha}$(M´´)), gray squares; ε''_{deriv} analysis ($\tau_\alpha(\varepsilon''_{deriv})$), for the anhydrous sample, gray triangles; TMDSC measurements (τ_α), stars, and from σ´ spectra, τ_σ, filled circles (see text). The solid lines are the VFTH curves with parameters: –log(τ_0 /s) = 17.7 ± 0.1, B = 1860 ± 42 K and T_0 = 134.5 ± 0.8 K for [C_2OHmim][Ibu]$_{18.5\%}$ (blue line) and –log(τ_0 /s) = 9.9 ± 0.3, B = 638 ± 67 K and T_0 = 226 ± 2 K for anhydrous [C_2OHmim][Ibu] (red line). The vertical dashed lines indicate the calorimetric glass transition temperatures for anhydrous and 18.5% samples.

For the latter the location of τ_α and τ_σ in the relaxation map (not shown) is the same observed for other molecular glass formers[47], for which τ_σ is significantly retarded relative to τ_α. Therefore the relative position of the conductivity and structural relaxation traces for [C_2OHmim][Ibu] in the relaxation map compared with Ibuprofen may be a manifestation of its greater water solubility.

IV. Conclusions

[C_2OHmim][Ibu] was produced by the adequate combination between a biocompatible 1-ethanol-3-methylimidazolium cation with the ibuprofenate anion derived from the almost water insoluble pharmaceutical drug ibuprofen. It was found that this combination turns the material highly hydrophilic with an increment of water solubility of around 5 orders of magnitude. The compound in the anhydrous form and with different water contents (3 and 18.5% w/w) was investigated by dielectric relaxation spectroscopy. Several relaxation processes were detected originated by dipolar reorientations, as found in conventional glass formers, to which conductivity also contributes, as observed for ionic conductors; thus [C_2OHmim][Ibu] exhibits a mixed behavior. The α-process associated with the dynamical glass transition is highly coupled with conductivity, in a more extent in the anhydrous material, so the dominant relaxation when data is analyzed in the modulus formalism was designated σα-process. The structural relaxation times were derived from permittivity analysis and confirmed by temperature modulated differential scanning calorimetry. The σα-process is highly sensitive to the water content, shifting to lower temperatures upon hydration. This was also observed for the calorimetric glass transition that shifts from -76.9°C (18.5% w/w water) to -21.3°C (anhydrous).

Ionic conduction increases with water content indicating that the presence of water not only has a plasticizing effect as well as enhances the ion conduction at the corresponding T_g.

At the lowest temperatures and higher frequencies a relaxation originated by dipolar fluctuations was detected, γ-process, associated with very local mobility that remains active deeply in the sub-T_g region. At intermediated frequencies it is detected a relaxation coherent with a β Johari-Goldstein (β_{JG}) process, which temperature dependence bents off near the glass transition temperature. This process is highly sensitive to the water content in both intensity and temperature location. In the relaxation map, the separation between σα and β_{JG} process highly decreases from the sample with 18.5 to the one with 3%; in the anhydrous form is hardly detected becoming largely hidden by the prominent σα-process. The closeness between the two processes in the less hydrated samples may contribute to the high tendency for crystallization, since it is assumed that secondary processes, intermolecular in nature, play a role in governing crystallization.

[C_2OHmim][Ibu] used here as a model compound, allowed to explore concepts under a more fundamental point of view but strongly pointing to useful applications in the pharmaceutical industry. Since several pharmaceutical drugs are administrated as aqueous formulations, these findings indicate that the combination of ibuprofen with the cation of the ionic liquid is a promissory strategy to obtain a more soluble and permeable Ibuprofen derived drug.

V. Acknowledgements

Financial support is acknowledged to Fundação para a Ciência e Tecnologia (FCT, Portugal) through the projects PTDC/CTM/098979/2008, PTDC/EQU-EPR/104554/2008 and

PTDC/CTM-NAN/120658 /2010. M. T. Viciosa acknowledges FCT for a post-doctoral grant SFRH/BPD/39691/2007.

VI. References

[1] H. D. Williams, N. L. Trevaskis, S. A. Charman, R. M. Shanker, W. N. Charman, C. W. Pouton and C. J. H. Porter, *Pharm. Rev.*, 2013, **65**, 315–499.

[2] L. Di, E. H. Kerns and G. T. Carter, *Curr. Pharm. Des.*, 2009, **15**, 2184–2194.

[3] L. Di and E. H. Kerns, Drug-like properties: concepts, structure design, and methods: from ADME to toxicity optimization, Elsevier, 2008.

[4] J. Stoimenovski, D. R. MacFarlane, K. Bica and R. D. Rogers, Pharm. Research, 2010, **27**(4), 521–526.

[5] W. L. Hough, M. Smiglak, H. Rodriguez, R. P. Swatloski, S. Spear, D. T. Daly, J. Pernak, J. E. Grisel, R. D. Carliss, M. D. Soutullo, J. H. Davis and R. D. Rogers, *New J. Chem.*, 2007, **31**, 1429–1436.

[6] R. Ferraz, L. C. Branco, C. Prudencio, J. P. Noronha and Z. Petrovski, *Chem. Med. Chem.*, 2011, **6**, 975–985.

[7] V. Kumar, V. Malhotra Sanjay, in Ionic Liquid Applications: Pharmaceuticals, Therapeutics, and Biotechnology, American Chemical Society, Washington, DC, 2010, pp. 1–12.

[8] M. A. Filippa and E. I. Gasull, *Fluid Phase Equilibria*, 2013, **354**, 185–190.

[9] J. Ranke, A. Othman, P. Fan and A. Müller, *Int. J. Mol. Sci.*, 2009, **10**, 1271–1289.

[10] R. F.M. Frade, A. A. Rosatella, C. S. Marques, L. C. Branco, P. S. Kulkarni, N. M. M. Mateus, C. A. M. Afonso, C. M.M. Duarte, *Green Chem.*, 2009, **11** (10), 1660–1665.

[11] E. Carignani, S. Borsacchi, M. Geppi, *J. Phys. Chem.* A, 2011, **115**, 8783–8790.

[12] F. Kremer and S. A. Rózanski, "The Dielectric Properties of Semiconducting Disordered Materials," in Broadband Dielectric Spectroscopy; Kremer, F.; Schönhals, A., Eds.; Springer Verlag: Berlin, 2003; Chapter 12.

[13] McCrum N. G., Read B. E. and Williams G., Anelastic and Dielectric Effects in Polymeric Solids, 1967, pp. 108–111.

[14] P. B. Macedo, C. T. Moynihan and R. Bose, *Phys. Chem. Glas.*, 1972, **13**, 171–179.

[15] M. Wübbenhorst and J. van Turnhout, *J. Non. Cryst. Solids*, 2002, **305**, 40–49.

[16] F. S. Howell, C. T. Moynihan and P. B. Macedo, *Bull. Chem. Soc. Jpn.*, 1984, **57**, 652–661.

[17] K. Pathmanathan and G. P. Johari, *J. Chem. Phys.* **1991**, 95, 5990–5998.

[18] E. Donth, Relaxation Dynamics in Liquids and Disordered Materials, Springer Series in Materials Science, Vol. 48, Berlin, 2001.

[19] Ngai, K. L. Relaxation and Diffusion in Complex Systems; Springer: New York, 2011; Chapter 2 and references therein.

[20] A. Rivera and E. Rössler, *Phys. Rev. B*, 2006, **73**, 1–4.

[21] T. Carvalho, V. Augusto, A. Rocha, N. M. T. Lourenço, N. Correia, S. Barreiros, P. Vidinha, E. Cabrita and M. Dionísio, *J. Phys. Chem. B*, 2014, **118**, 9445–9459.

[22] K. L. Ngai and M. Paluch, *J. Phys. Condens. Matter*, 2003, **15**, S1107–1125.

[23] M. Mathlouthia and J. Genotelleb, *Carbohydr. Polym.*, 1998, **37**, 335–342.

[24] Z. Wojnarowska, K. Grzybowska, L. Hawelek, A. Swiety-Pospiech, E. Masiewicz, M. Paluch, W. Sawicki, A. Chmielewska, P. Bujak and J. Markowski, *Mol. Pharmaceutics*, 2012, **9**, 1250–1261.

[25] A. Schönhals and F. Kremer, "Analysis of Dielectric Spectra" in Broadband Dielectric Spectroscopy; Kremer, F.; Schönhals, A., Eds.; Springer Verlag: Berlin, 2003; Chapter 3.

[26] G. Polizos, E. Tuncer, V. Tomer, I. Sauers, C. A. Randall and E. Manias, "Dielectric Spectroscopy of Polymer-Based Nanocomposite Dielectrics with Tailored Interfaces and Structured Spatial Distribution of Fillers", in Nanoscale Spectroscopy with Applications, 2013, S. M. Musa, Ed. 2013.

[27] H. Vogel, *Phys. Zeit.*, 1921, **22**, 645–646.

[28] G. S. Fulcher, *J. Am. Ceram. Soc.*, 1925, **8**, 339-355.

[29] G. Tammann and W. Hesse, *Z. Anorg. Allg. Chem.*, 1926, **156**, 245–257.

[30] P. G. Debenedetti, Metastable Liquids: Concepts and Principles, Princeton University Press, Princeton, New Jersey, 1996; Chapter 4.

[31] A. K. Jonscher, *Nature*, 1977, **267**, 673–679.

[32] T. Carvalho, V. Augusto, A. R. Brás, N. M. T. Lourenço, C. A. M. Afonso, S. Barreiros, N. T. Correia, P. Vidinha, E. J. Cabrita, C. J. Dias, M. Dionísio, B. Roling, *J. Phys. Chem. B*, 2012, **116**, 2664–2676.

[33] S. V. Troshenkova, E. S. Sashina, N. P. Novoselov, K. F. Arndt and S. Jankowsky, *Russ. J. Gen. Chem.*, 2010, **80**, 106–111.

[34] J. G. Huddleston, A. E. Visser, W. M. Reichert, H. D. Willauer, G. A. Broker and R. D. Rogers, *Green Chem.*, 2001, **3**, 156–164.

[35] Z. Wojnarowska, K. Kołodziejczyk, K. J. Paluch, L. Tajber, K. Grzybowska, K. L. Ngai and M. Paluch, *Phys. Chem. Chem. Phys.* 2013, **15**, 9205–9211.

[36] H. Diogo and J. J. Moura Ramos, *J. Polym. Science: Part B: Polym. Phys.*, 2009, **47**, 820–829.

[37] N. Shinyashiki, M. Shinohara, Y. Iwata, T. Goto, M. Oyama, S. Suzuki, W. Yamamoto, S. Yagihara, T. Inoue, S. Oyaizu, S. Yamamoto,K. L. Ngai and S. Capaccioli, *J. Phys. Chem. B*, 2008, **112**, 15470–15477.

[38] A. Kudlik, C. Tschirwitz, T. Blochowicz, S. Benkhof and E. Rössler, *J. Non-Cryst. Solids*, 1998, **235-237**, 406-411.

[39] K. L. Ngai and S. Capaccioli, *Phys. Rev. E*, 2004, **69**, 031501 (1–5).

[40] N. T. Correia and J. J. Moura Ramos, *Phys. Chem. Chem. Phys.*, 2000, **2**, 5712–5715.

[41] P. A. M. Steeman and J. van Turnhout, "Dielectric Properties in Inhomogeneous Media" in Broadband Dielectric Spectroscopy; Kremer, F.; Schönhals, A., Eds.; Springer Verlag: Berlin, 2003; Chapter 13.
[42] S. Summerfield, *Philos. Mag. B - Phys. Conden. Mat. Stat. Mech. Electr. Opt. Magn. Prop.*, 1985, **52**, 9–22.
[43] T. M. Chang, L. X. Dang, R. Devanathan and M. Dupuis, *J. Phys. Chem. A*, 2010, **114**, 12764−12774.
[44] C. T. Moynihan, N. Balitactac, L. Boone and T. A. Litovitz, *J. Chem. Phys.*, 1971, **55**, 3013−3019.
[45] J. R. Sangoro, C. Iacob, A. Serghei, C. Friedrich and F. Kremer, *Phys. Chem. Chem. Phys.*, 2009, **11**, 913–916.
[46] B. Roling, Charge Transport in Disordered Solids with Applications in Electronics, in Mechanisms of Ion Transport in Amorphous and Nanostructured Materials, John Wiley, Baranovski S., 2006, p. 382.
[47] M. Köhler, P. Lunkenheimer and A. Loidl. *Eur. Phys. J. E*, 2008, **27**, 115–122.